DOI: 10.1002/ ((please add manuscript number))
Article type: Full Paper

Enzyme-Powered Nanobots Enhance Anticancer Drug Delivery

Ana C. Hortelão †, // , Tania Patiño †, // *, Ariadna Perez-Jiménez †, Àngel Blanco † and Samuel Sánchez †, // ,‡*

† Institute for Bioengineering of Catalonia (IBEC), The Barcelona Institute of Science and Technology, Baldiri Reixac 10-12, 08028 Barcelona Spain

// Max Planck Institute for Intelligent Systems Institution, Heisenbergstraße 3, 70569 Stuttgart, Germany.

‡ Institució Catalana de Recerca i Estudis Avancats (ICREA), Pg. Lluís Companys 23, 08010, Barcelona, Spain

*e-mail: ssanchez@ibecbarcelona.eu, tpatino@ibecbarcelona.eu

Keywords: nanobots, nanomachines, enzymatic catalysis, drug delivery, nanomotors

The use of enzyme catalysis to power of micro- and nanomotors exploiting biocompatible fuels has opened new ventures for biomedical applications such as the active transport and delivery of specific drugs to the site of interest. Here, urease powered nanomotors (nanobots) for the doxorubicin (Dox) anti-cancer drug loading, release and efficient delivery to cells are presented. These mesoporous silica-based core-shell nanobots are able to self-propel in ionic media, as confirmed by optical tracking and dynamic light scattering analysis. A four-fold increase in drug release is achieved by nanobots after 6 hours compared to their passive counterparts.

Furthermore, the use of Dox-loaded nanobots presents an enhanced anti-cancer efficiency towards HeLa cells, which arises from a synergistic effect of the enhanced drug release and the ammonia produced at high concentrations of urea substrate. A higher content of Dox inside HeLa cells is detected after 1, 4, 6 and 24 hours incubation with active nanobots compared to passive dox-loaded nanoparticles. The improvement in drug delivery efficiency achieved by enzyme-powered nanobots may hold potential towards their use in future biomedical applications such as the substrate-triggered release of drugs in target locations.

1. Introduction

The design of active and smart systems capable of bypassing side effects while increasing drug efficacy is a long-standing challenge in biomedicine and nanotechnology. Such systems require a number of characteristics, namely biocompatibility, biodegradability, and circulation stability. Furthermore, their maneuvering for full motion control is required to be able to deliver cargo at the defined locations, minimizing undesirable effects in the bystander tissues.[1–3]

Traditional drug delivery systems rely on the use of passive nanoparticles (i.e. without propulsion capabilities), which has been reported to have low efficacy.[2] In contrast, in the last decade, researchers have developed micro-/nanoparticles able to self-propel in aqueous media, which have potential as novel and active drug delivery vehicles.[4–9] Propulsion at the micro-/nanoscale can be achieved by a multitude of approaches, such as the use of ultra-sound waves,[10] light,[11,12] magnetic fields,[13,14] by coupling motile cells to particles[15–21] or by catalytic decomposition of a chemical substrate.[22–25] Since catalytic micro-/nanomotors were primarily based on the use of toxic fuels, such as hydrogen peroxide[26–29] and hydrazine,[30] the potential of these synthetic motors in the biomedical field demanded the quest for alternative biocompatible fuel sources. Alternatively, the use of enzymes as biological catalytic units to power the motion of varied micro-/nanostructures has been reported.[22,31–37] Enzyme catalysis presents several advantages as compared to other catalytic motors. For instance, enzymes

provide a more versatile library of relevant, bioavailable and biocompatible substrates to be used as fuels upon demand of the target application.

The self-propulsion abilities of these synthetic motors may bring distinct improvements when compared to passive drug carriers. Namely, self-propulsion provides the vehicles with continuous driving force, aiding their transport across biological tissues.[5,38] In addition, upon regulation of the motors' speed, cell targeting and internalization phenomena could be modulated, providing enhanced control and tunability of the drug delivery system.[39] Considerable efforts have been applied to the fabrication of micro-/nanomotors that fulfil the requirements for ideal drug delivery vehicles.[31,32,40–42] Mesoporous silica, specifically the Mobil Composition of Matter No. 41 (MCM-41) type, is a widely studied material for biomedical applications which is approved for clinical use by the FDA.[43,44] Previous research on this type of silica revealed it to be biocompatible, which in addition to its high cargo loading capacity, tunability, and easy surface chemistry make it an optimal chassis for drug delivery vehicles.[44] Our group previously demonstrated the self-propulsion of micro- and nanostructures based on MCM-41 silica and their coupling with enzymes to engineer nanomotors powered by the bio-catalytic conversion of urea and glucose, aiming at their application in the biomedical field.[31,32,45,46] However, the benefits in drug delivery based on active particles compared with passive particles, as well as their motion in physiological media has not been reported yet.

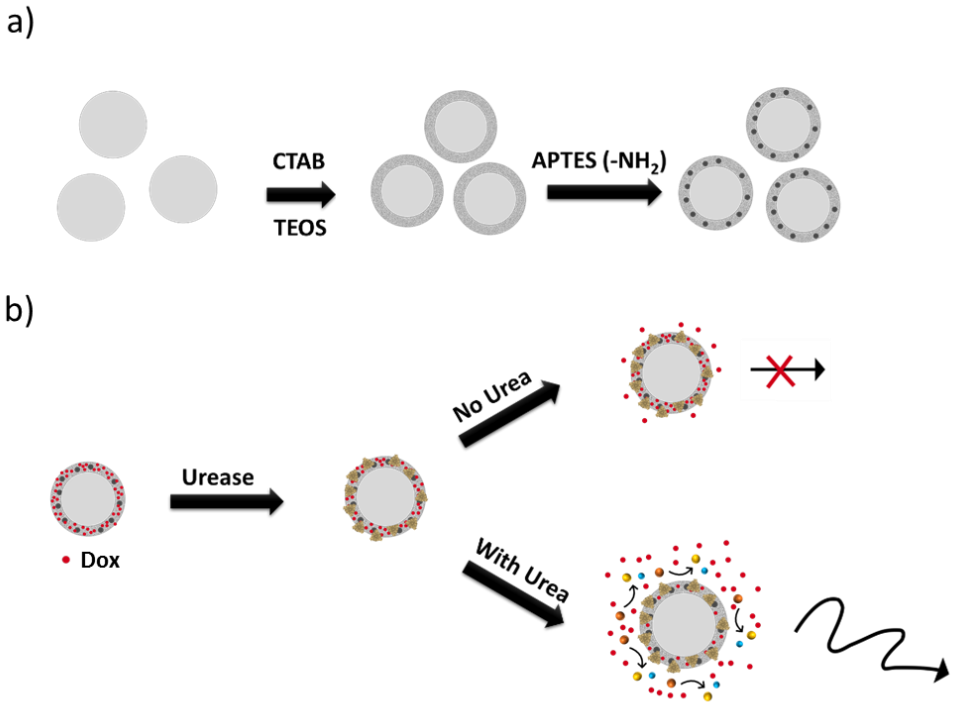

Scheme 1. Schematic illustration of the fabrication and drug delivery system features of the urease nanobots. Fabrication of the nanobot mesoporous structure using cetyltrimethylammonium bromide (CTAB) and tetraethylorthosilicate (TEOS), and further modification with amine groups using 3-aminopropyltriethoxysilane (APTES) (a). Loading of Doxorubicin (Dox) onto the mesoporous shell, urease attachment and enhanced drug release provoked by self-propulsion due to the presence of urea (b).

Herein, we present the facile fabrication of enzymatic nanomotors, dubbed nanobots, comprised of a solid silica core and a mesoporous silica shell (Scheme 1a). The shell was coated with urease enzymes which allows to harness chemical energy and convert it into mechanical work even in ionic media (PBS buffer solution), an important characteristic for their potential use in biomedical applications. Furthermore, the mesoporous shell provides high loading capacity, enabling the retention of the anti-cancer water-soluble drug Doxorubicin (Dox) (Scheme 1b) and its active transport towards cancer cells. The presence and release of Dox inside the cell is quantified and imaged by fluorescence microscopy.

2. Results and discussion

2.1. Synthesis and characterization of the urease nanobots

Solid silica spheres, synthesized using a modified Stöber method,[47] were used as core for the fabrication of core-shell nanoparticles (MSNP), as depicted in Scheme S1. The mesoporous silica shell was grown based on previously reported approaches that provide stability and low aggregation in solution.[31] We used cetyltrimethylammonium bromide (CTAB) as porogenic agent and triethanolamine (TEOA) as a base catalyst (see experimental details in the Methods section). The MSNP were functionalized with 3-aminopropyltriethoxysilane (APTES) to obtain nanoparticles with free amine groups on the surface (MSNP-NH_2), which were used to covalently attach urease to the nanoparticles using glutaraldehyde (GA) as linker molecule, thus yielding urease nanobots. The fabrication process was characterized by scanning electron microscopy (SEM) and dynamic light scattering (DLS). **Figure 1a** displays SEM micrograph of MSNP, revealing the good monodispersity of the MSNPs (Ø = 344 ± 3, average size ± standard error of mean (SE), N = 60). DLS analysis of the hydrodynamic radius showed a single population distribution, indicating that the particles were not aggregated, even after their functionalization with APTES. After urease attachment, however, a slightly broader peak than the one detected for the MSNP-NH_2 was observed, indicating a lower monodispersity of the particles in terms of hydrodynamic radius, which could be attributed to enzyme conjugation (Figure 1b, green). Furthermore, we evaluated the evolution of the surface charge upon the modifications of the as-synthesized MSNPs (Figure 1c), denoting negative surface charge for the MSNPs (-16.5 ± 1.4 mV, average ± SE, N = 9) and a clear shift to positive surface charge after amine modification (43.5 ± 0.4 mV, average ± SE, N = 9). Moreover, we observed a sharp decrease on the positively charged surface after the functionalization with urease enzyme (10.3 ± 1.0, average ± SE, N = 9) (Figure 1c). Since urease has an isoelectric point between 5.0 and 5.2, the observed decrease on the surface charges could be attributed to a successful binding of urease enzyme to the particles.[48] The porosity and structure of the nanobots were analyzed by Transmission Electron Microscopy (TEM). We observed a clear core-shell structure (Figure 1d-f), where the nanochannels formed upon CTAB removal can be clearly distinguished (Figure

1f). The presence of urease enzyme on the particles' surface, as well as the elimination of unbound enzymes was analyzed through the use of a colorimetric kit based on reduction of copper by proteins' peptide bonds (Figure S1). [49]

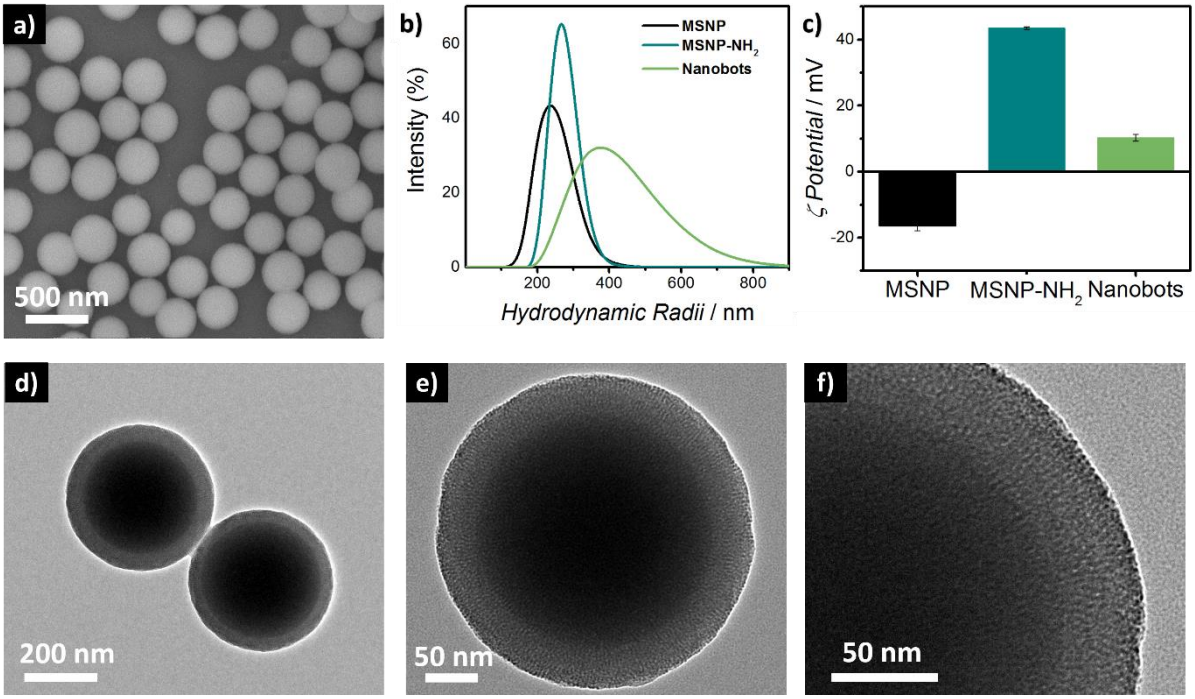

Figure 1. Characterization of the mesoporous silica nanoparticles (MSNP) and further modifications to obtain the mesoporous silica nanoparticles functionalized with urease (nanobots). SEM micrograph of MSNPs (a). Hydrodynamic radii (b) and surface charge evolution (c) upon surface modification of the mesoporous silica nanoparticles with amine functional groups and further with urease enzyme. TEM micrographs of MSNP-NH_2 (d), evidencing the core-shell structure (e) and porosity features (f) of the nanoparticles.

2.2. Motion behavior of urease nanobots

In the presence of urea, the urease bound to the surface of the nanobots catalyzes the decomposition of urea into ammonia and carbon dioxide [(NH2)2CO + H2O → CO2 + 2 NH3]. As previous reports have shown, enzymatic catalysis can be used to achieve self-propulsion of micro- and nanostructures with different architectures.[22,31,34,36,45] Some nanomotors have been fabricated by inducing structural asymmetries such as the creation of Janus particles[31,32] or other asymmetric shapes such as polymeric stomatocytes.[34] However, other studies have reported an enhanced diffusion for non-Janus spherical polystyrene particles.[50] The actual mechanism of motion for enzymatic motors is still under debate.[32,33,35,37,51,50,52] The self-

propelling abilities of the nanobots due to the presence of urea was characterized by optical tracking of the nanobots trajectories under a range of urea concentrations **(Figure 2a)**. The mean-squared displacement (MSD) resulting from the tracked trajectories (Figure 2b) increases linearly with time, which is typical of diffusive motion.[53] The effective diffusion coefficient (D_e) was obtained by fitting the MSD curves to equation 1:

$$MSD(\Delta t) = 4 \cdot D_e \cdot \Delta t, \quad (1)$$

where D_e represents the effective diffusion coefficient and Δt represents the time interval.[54]

The calculated effective diffusion coefficients are represented in Figure 2c, blue. We further confirmed these results by analysing the diffusion coefficients of nanobots in the presence of urea by DLS (Figure 2c, green). In both cases a significant increase in the effective diffusion coefficient was observed at a 25 mM urea concentration ($p < 0.05$), which was further increased at 50 mM urea, reaching a stabilization. The stabilization of the diffusion coefficient values in the presence of increasing concentrations of urea can be explained by the activity kinetics of urease. We evaluated the activity of the covalently bound urease on the nanobots surface, over the range of urea concentrations studied for motion and we observed that the nanobots present Henri-Michaelis-Menten kinetics (Figure 2d), obeying equation 2:

$$v = \frac{V_{max}[S]}{K_m + [S]}, \quad (2)$$

where V_{max} represents the maximum reaction rate, S represents the urea concentration and K_m represents the Henri-Michaelis-Menten constant.[55] By fitting our data to the equation, we found that K_m = 4.7 ± 0.5 mM and V_{max} = 162.1 ± 1.5 units/mg of urease, where unit is defined as the amount of enzyme required to generate 1 μmol of ammonia per minute, at 37 °C and pH 7.0. These results are in good agreement with values for free enzyme found in literature, indicating that urease activity was not affected by its functionalization onto the particles. [56]

We further characterized the activity of urease enzyme present on the nanobots' surface over a period of 120 minutes, denoting that the enzymatic rate decreases continually with time (inset

of Figure 2d), suggesting that the consumption of substrate and generation of products slows the reaction rate over time.

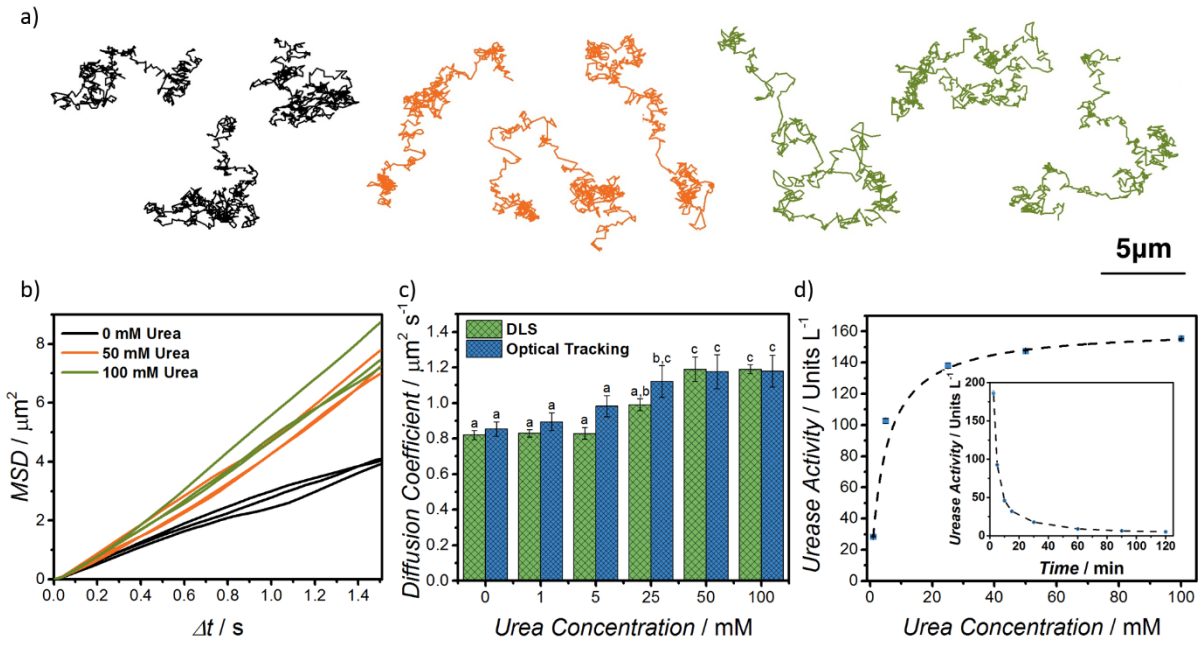

Figure *2*. Analysis of the motion behavior of urease nanobots. Representative tracking trajectories of urease nanobots with different urea concentrations (0 mM – black, 50 mM – orange and 100 mM - green) (a) and correspondent mean-squared displacement (MSD) plots (b); Effective diffusion coefficient obtained by analyzing the MSD (blue) and by DLS (green) of urease nanobots at different urea concentrations (n=20, error bars represent SE) (c). Different superscripts denote significant differences among groups with $p < 0.05$; Enzymatic activity of the urease nanobots at different urea concentrations fitted to Henri-Michaelis-Menten equation (inset: variation of enzymatic activity of the nanobots with time) (d).

Motivated by the intrinsic presence of salts in physiologically relevant media, we investigated the effect of the presence of salts in the surrounding medium on the nanobots' diffusion coefficient, using phosphate buffered saline solution (PBS 1x). We observed different diffusion coefficient values between nanobots suspended in water and in PBS **(Figure 3a)**, which could be attributed to changes in electrostatic interactions between motors and neighboring surfaces driven by the presence of salts.[57] However, the nanobots displayed enhanced diffusion in both PBS and water solutions in the presence of urea, where an increase in diffusion coefficient of roughly 35% and 60% was detected for water and PBS, respectively (Figure 3b). We also

analyzed the nanobots self-propulsion in ionic media by DLS, where a shift on diffusion coefficient is observed (Figure 3c).

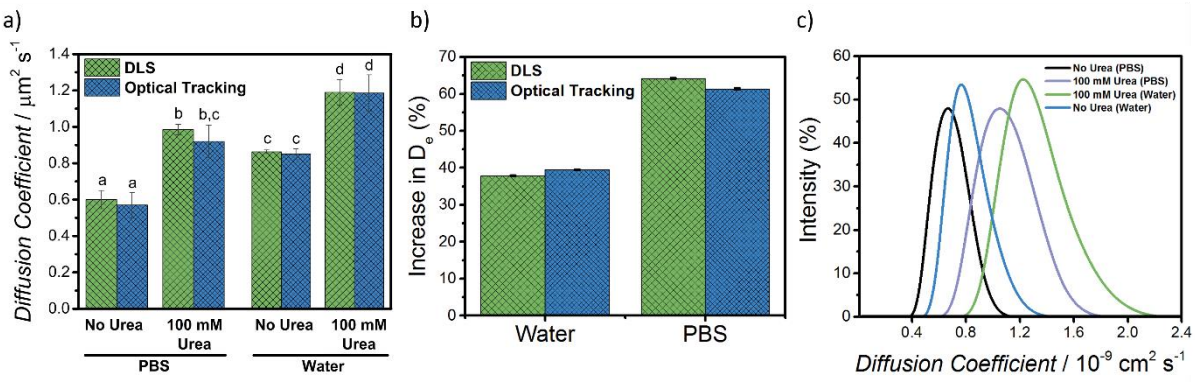

Figure 3. Analysis of motion behaviors of urease nanobots in water and ionic media. Characterization of the motion profiles of urease-powered nanobots in ionic media (PBS) and in water by optical microscopy and DLS (N=20, error bars represent SE) (a). Different superscripts denote significant differences among groups with $p < 0.05$. Percentage increase in diffusion coefficient in the presence of urea, in water and in PBS, error bars represent the error calculated by propagating the SE obtained in the measurements (b). Diffusion coefficient histogram nanobots in water and PBS obtained by DLS (c).

2.3. Drug loading and release profiles of the urease nanobots

We investigated the drug loading and releasing capabilities of nanobots in order to determine whether their enhanced diffusion due to availability of urea relates with enhanced drug release kinetics. First, we investigated the loading capacity of the architecture of the nanobots before and after functionalizing with urease enzyme as drug delivery carrier, using Dox as model drug. Dox is a chemotherapeutic agent which belongs to the family of anthracyclines and antitumor antibiotics, which intercalates between the base pairs in the DNA, preventing replication and thereby arresting the cell cycle.[58] We determined nanobots' loading capacity and drug entrapment efficiency, which represent the drug content and the percentage of drug successfully encapsulated in the nanoparticles, respectively, as follows

$$Drug\ Loading\ (\%) = \frac{Mass\ of\ Drug\ Loaded}{Mass\ of\ Nanobots} \times 100 \qquad (3)$$

$$Entrapment\ Efficiency\ (\%) = \frac{Mass\ of\ Drug\ Loaded}{Total\ Drug\ Mass} \times 100 \qquad (4)$$

Despite a slight loss of Dox mass during the washing process required for functionalization with urease, the nanobots retain roughly 10 % (w/w) of drug **(Figure 4a)**.

Then, we compared the drug release capabilities of enzymatic nanobots in the presence of increasing concentrations of fuel with their passive counterparts (Figure 4b and c). We observed that the drug release over 24h hours increased according to the presence of urea. A positive correlation between the urea concentration and the release profile was found, reaching a saturation at 50 mM urea. The amount of Dox released by the nanobots at urea concentrations above 50 mM is almost four times higher compared to the one obtained at 0 mM urea (Figure 4b). These results are in agreement with the motion analysis, since the saturation of motion was also found to be 50 mM of urea. We attribute the enhancement of the drug release from the mesoporous cavities to the increased diffusion of the nanobots in the presence of urea, and to the flow generated through the surface.[33,59] Since we observed that urease activity decreases overtime (Figure 2d), we performed the release experiments collecting aliquots at every time point and replenishing the medium with fresh supply of urea. Thus, the slow release rate between 6 and 24h, observed for all conditions analyzed, could be explained by the depletion of urea from the medium, as well as by the saturation of the solution with Dox, slowing down the drug release.

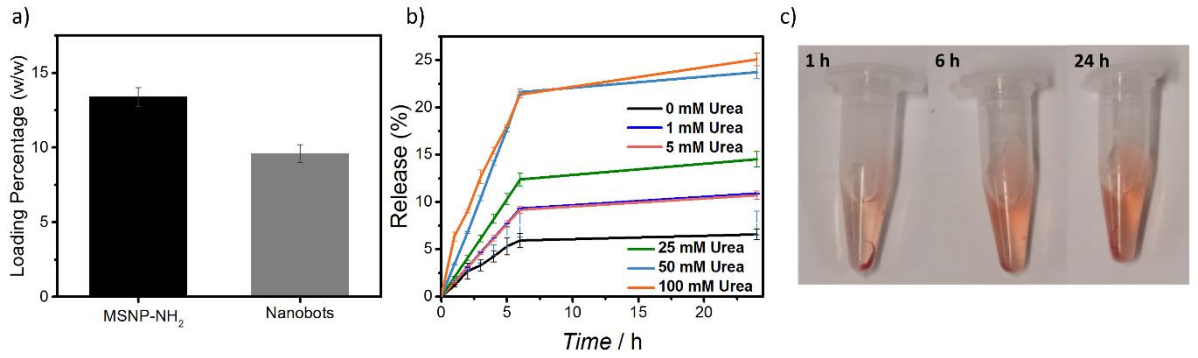

Figure 4. Evaluation of MSNP-NH_2 and urease nanobots as drug carriers for Dox. a) Loading capacity of Doxorubicin on MSNP-NH_2 and urease nanobots; b) Release profiles for Dox from the nanobots in different urea concentrations (N = 3, error bars represent SE) and c) Release of Dox from nanobots in the presence of 100 mM urea.

To study whether the changes in the Dox release profiles could be affected by the changes in the pH provoked by urease activity, we monitored the pH of the nanobots solution upon the addition of urea. For this, we used PBS adjusted to different pH (5, 6, 9 and 10) as the starting solutions, and the pH was measured every minute upon the addition of urea. We observed that in all cases, the pH changed immediately to 9, indicating the self-buffering properties of the system (Figure S3a). To assess if the quick change in pH was the reason underlying the enhancement on drug release, we evaluated the release profiles of nanobots in the presence and absence of urea, when placed in buffer solutions at pH 9 (Figure S3b). We observed that even when the initial solution was stabilized at pH 9, the release of Dox from the urease nanobots was significantly enhanced in the presence of urea, indicating that this phenomenon stems from nanobots' surface activity, regardless of the pH change of the surrounding medium.

2.4. Nanobots' efficacy as drug delivery vehicles

Taking advantage of the enhanced Dox release kinetics from active nanobots, we tested nanobots' biocompatibility and efficacy as drug delivery vehicles to human epithelial cervix adenocarcinoma HeLa cells. Urease-powered nanobots' biocompatibility was evaluated by using the (3-(4,5-dimethylthiazol-2-yl)-2,5-diphenyltetrazolium bromide (MTT) assay, which is a colorimetric method that determines metabolic activity, by assessing the reduction of MTT and formation of formazan crystals by viable cells. The nanobots exhibited biocompatibility (>80% viable cells) up to a concentration of 0.5 mg/mL (**Figure 5a**, black), where less than 70% of the cells remained viable after the 24 hours incubation period. Viability below that value would denote cytotoxicity of nanoparticles, as per the FDA's and ISO's standards.[60] When nanobots were loaded with Dox and incubated with cells (even in the absence of urea) we observed a concentration-dependent toxicity trend, which was significantly higher than non-Dox loaded nanobots in all cases (Figure 5a, blue). A concentration of 4 µg/ml of free Dox is needed to achieve the IC50 on HeLa cells after 24 hours incubation (Figure S3). Using core-

shell nanoparticles, we evaluated IC50 resulting that 0.5 mg/ml of passive nanobots (concentration of Dox loaded = 48 µg/mL), whereas only 0.05 mg/ml of active nanobots are required to obtain the same effect. These results indicate that not all the loaded Dox encapsulated in passive nanobots is released or capable of reaching the desired location, i.e. inside the cells. Yet, once urea is present in the medium, a more efficient delivery of Dox to the cells is achieved, which could be attributed to a faster release of drug to the media, increased transport near or inside the cell and increased cell uptake of the nanobots. The exact contribution from each effect needs to be investigated in future works.

Figure 5 b (green columns) shows the anti-cancer effect of Dox-loaded active nanobots, which was attributed to the enhanced release of Dox from active nanobots for increasing concentrations of urea. Moreover, we observed a sharp decrease in cell viability for bare nanobots for concentrations above 10 mM of urea (Figure 5b, black columns). To investigate the origin of this low viability, we studied the cytotoxic contribution of fuel and products, we evaluated the biocompatibility of urea and ammonia. Urea was found to be biocompatible for concentrations up to 400 mM (Figure S5a). Yet, we observed a cytotoxic effect for ammonia concentrations higher than 50 mM (Figure S5b), which would correspond to the total conversion of 25 mM urea.

Altogether, these results indicate that, as a matter of comparison, we obtain the same effect on cells with at least ten times lower concentration of active nanobots than with passive counterparts. We attribute these results to a synergistic effect of the improved Dox release induced by motion, and the ammonia produced by catalytic decomposition of urea.

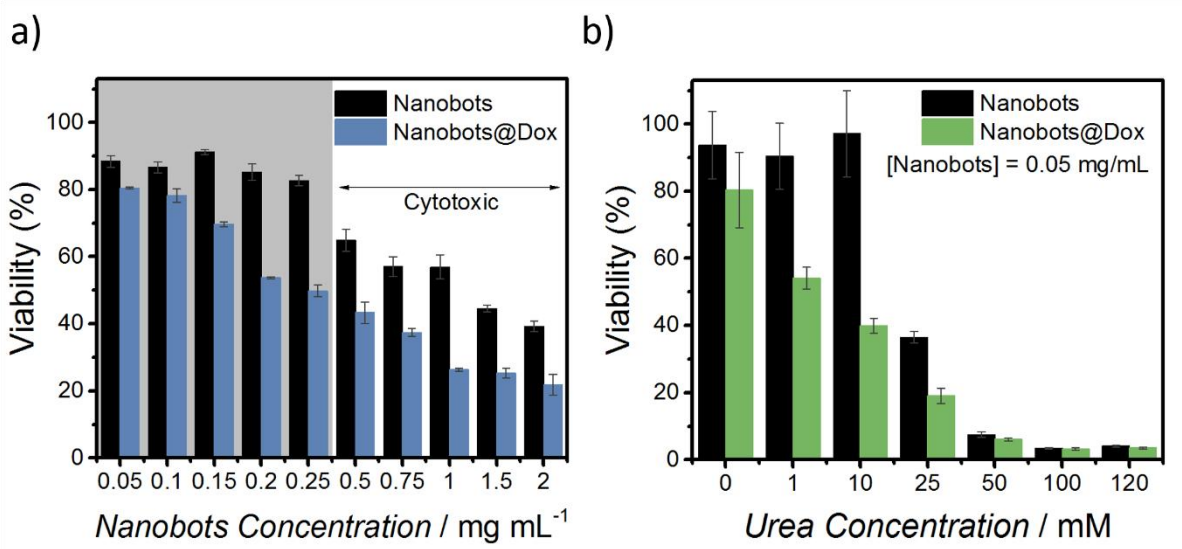

Figure 5. Cytotoxicity assays and efficacy testing of the nanobots as drug carriers in the presence and absence of urea. Biocompatibility of nanobots (black) up to high concentrations and evaluation of its efficacy as Dox carrier (blue) without urea (a); Urea-dependent biocompatibility of the urease nanobots (black) and increased efficacy as Dox delivery vehicles (green) at 0.05 mg/mL (b) (N=3, error bars represent SE).

As Dox is a fluorescent molecule, we used fluorescence microscopy to monitor its uptake by Hela cells **(Figure 6a)**. For this, cells were incubated with 0.05 mg/mL of Dox-loaded nanobots, either in the absence or presence of urea (10 mM) during 1, 4, 6 and 24 hours, after which the cells were washed with PBS and labeled with wheat germ agglutinin (WGA – membrane, green) and Hoescht (nuclei, blue). Next, quantitative imaging analysis of the red fluorescence emission within cells (Figure 6b, N = 15) was performed, observing that the fluorescence signal increases with time. Moreover, for all the data points analyzed, we observed a higher red fluorescence signal within cell cytoplasm when the nanobots were incubated with urea compared to the control, as depicted in Figure 6b and in Figure 6c (red channel column). These results agree with the findings from the cytotoxicity experiments, where active nanobots lead to an enhanced cytotoxic effect of the drug delivery system.

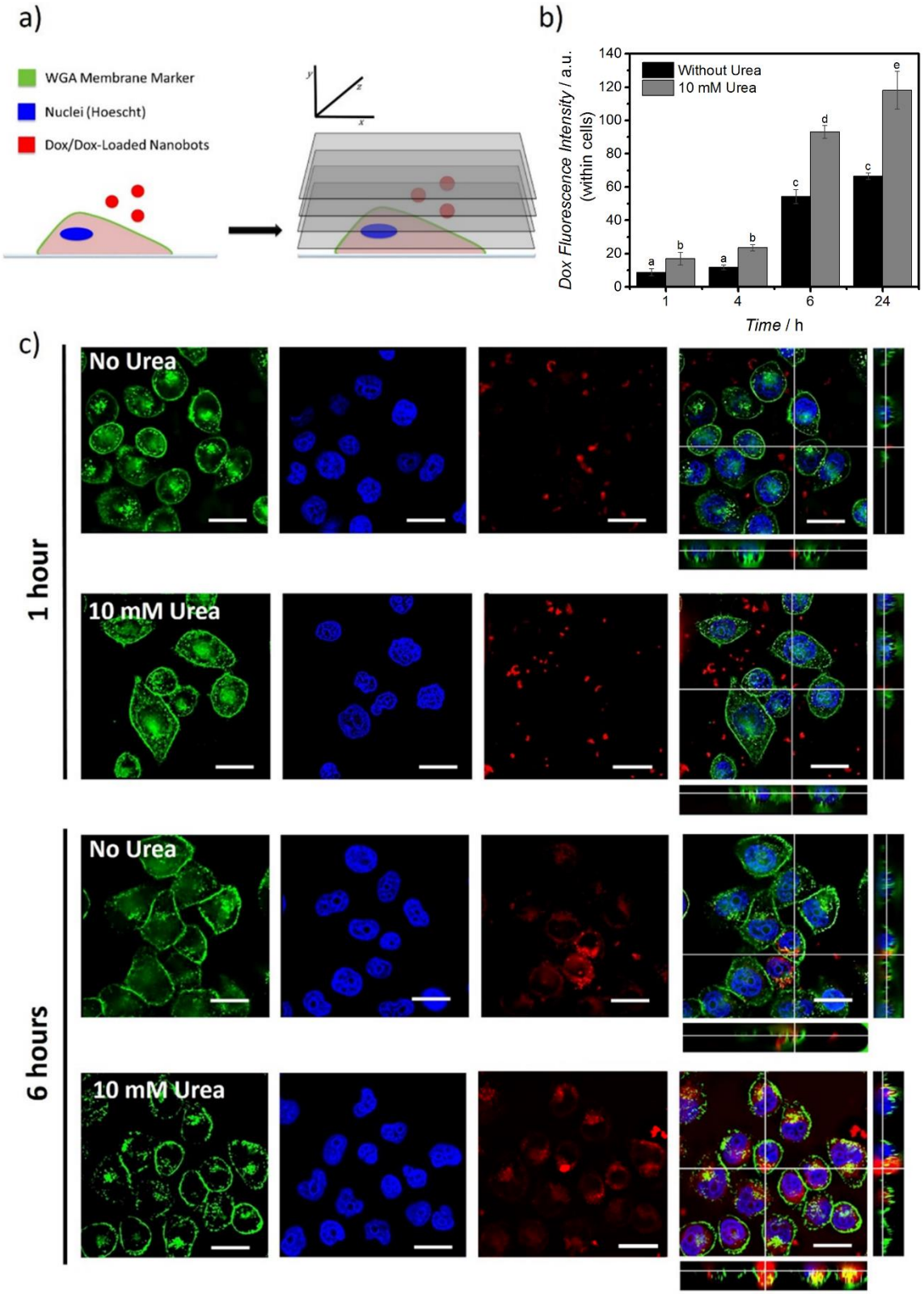

Figure 6. Interaction of Dox-loaded urease nanobots with HeLa cells. Schematic representing the cell labeling and imaging acquisition, Cell membranes were marked with wheat germ agglutinin (WGA, green), and nuclei were marked with hoescht (blue). red emission comes from Dox (a); Dox fluorescence emission quantification in regions within cells, in the absence (black) and presence of urea (grey) (N=15, error bars represent SE), different superscripts

denote significant differences among groups with $p < 0.05$ (b); Fluorescence imaging of HeLa cells and Dox-loaded nanobots (0.05 mg/mL). Scale bars are 20 μm (c).

3. Conclusion

In summary, we report urease-modified nanobots, composed of mesoporous silica shell, capable of loading the anticancer drug Dox, presenting enhanced drug release profiles dependent on urea concentration. Furthermore, we demonstrate the nanobots' self-propulsion in ionic media (PBS buffer), which is a crucial ability for its use in biomedical applications. We found that in the presence of urea, the active Dox-loaded nanobots exhibit improved effect on HeLa cells compared to passive carriers, due to a synergistic effect of improved drug release kinetics and ammonia production by the catalytic decomposition of urea. Future work on fuel-dependent targeting and cell uptake, novel triggered release mechanisms and *in situ* guidance methods, such as the use of pH, thermal or chemical gradients to attract and guide nanomotors *in vitro* and *in vivo* need to be addressed for the development of smart and self-propelled drug delivery vehicles based on enzyme catalysis.

4. Experimental Section ((delete section if not applicable))

Materials:

Ethanol (EtOH, >99%), Methanol (MeOH, >99%), Hydrochloric Acid (37% in water), Ammonium Hydroxide (25% in water), Tetraethylorthosilicate (TEOS, 99%), Triethanolamine (TEOA, 99%), Cetyltrimethylammonium bromide (CTAB, 99%), 3-Aminopropyltriethoxysilane (APTES, 99%), Glutaraldehyde (GA, 25% in water), Urease (from Canavalia ensiformis, Type IX, powder, 50,000-100,000 units/g solid), Urease Activity Kit, Doxorubicin Hydrochloride (Dox, 99.9%), Urea (99.9%), and Dimethyl sulfoxide (DMSO, 99.9%) were purchased from Sigma-Aldrich. (3-(4,5-dimethylthiazol-2-yl)-2,5-diphenyltetrazolium bromide (MTT), phosphate buffer saline (PBS), and Dulbecco's Modified Eagle Medium (DMEM) were purchased from Thermo Fischer Scientific.

Instruments:

Transmission Electron Microscopy (TEM) images were captures by a JEOL JEM-2100 microscope. Scanning Electron Microscopy (SEM) images were captured by a FEI NOVA NanoSEM 230 at 5 kV. Hydrodynamic radii and electrophoretic mobility measurements were performed using a Wyatt Möbius coupled with an Atlas cell pressurization system. Absorbance spectra of Dox, protein quantification and enzymatic activity assays were carried out using an Infinite M200 PRO Multimode Microplate Reader. Optical videos were acquired using a Leica DMi8 inverted microscope equipped with a 63x water objective.

Synthesis of Solid SiO_2 Spheres:

The solid silica spheres were prepared using the modified Stöber method. [47] Briefly, a solution containing EtOH (7 mL), ultra-pure water (10 mL) and ammonium hydroxide (2 mL) was stirred for 15 minutes. After, TEOS (6 mL) was added dropwise and the mixture was kept stirring for 21 hours. The formed particles were then collected by centrifugation and washed with EtOH (3 times, 2348 g, 3.5 minutes). Finally, the spheres were suspended in EtOH and aliquots (0.5 mL) were collected, centrifuged, air dried and weighed to determine the concentration of the solid SiO_2 suspension.

Coating of Mesoporous Silica Shell on Solid SiO_2 Spheres:

Solid silica spheres (60 mg) were suspended in a solution containing water (20 mL), TEOA (40 mg) and CTAB (75 mg). The solution was heated to 80 °C and TEOS (0.125 mL) was added dropwise, while the solution was stirred. The mixture was kept stirring for 2 hours, after which it was collected by centrifugation (845 g, 2.5 minutes) and washed with ultra-pure water once. Following, the obtained particles were suspended ina solution of MeOH and HCl (30 mL, 10:0.6) and refluxed at 80 °C for 24 hours. Finally, the particles were collected by centrifugation (2.5 minutes, 845 g) and washed in EtOH (3 times) and ultra-pure water (3 times). Aliquots (0.5

mL) were collected, centrifuged, air dried and weighed to determine the concentration of the suspension.

Amine Functionalization of MSNP:

The obtained MSNP (2 mg mL^{-1}) were then suspended in EtOH:APTES mixture (20:1, v/v) and shaken during 24 hours on an end-to-end rotary shaker. After, the particles were collected by centrifugation (845 g, 2.5 minutes) and washed in 3 times with EtOH and 3 times with water. Aliquots (0.5 mL) were collected, centrifuged, air dried and weighed to determine the concentration of the suspension.

Urease Functionalization of MSNP-NH_2: MSNP-NH_2 (2 mg) were washed 3 times with PBS 1x. After, the MSNP-NH_2 were suspended in (0.9 mL) PBS and GA (100 µL, 25% in water) was added to the mixture. The mixture was thoroughly vortexed to ensure good dispersion and shaken during 2.5 hours on an end-to-end rotary shaker. Then, the particles were collected by centrifugation and washed 3 times with PBS. Afterwards, the MSNP-NH_2 activated with GA were suspended in a solution of PBS containing urease (3 mg mL^{-1}) and mixed end-to-end on a rotary shaker for 18 hours. The resulting urease nanobots were collected by centrifugation (1150 g, 3.5 minutes) and washed 3 times with PBS.

Dox Loading in MSNP-NH_2:

Aliquots of MSNP-NH_2 (1 mg) were suspended in a Dox solution at a concentration of 1 mM and vortexed thoroughly to ensure good dispersion. Then, the mixture was incubated during 24 hours at room temperature, mixing end-to-end on a rotary shaker. The Dox loaded MSNP-NH_2 were then collected by centrifugation (1150 g, 3.5 minutes) and washed 3 times with PBS to ensure complete removal of non-loaded drug. The supernatants were kept and analysed by measuring the absorbance at 480 nm, using an Infinite M200 PRO Multimode Microplate

Reader, to determine the drug loading capacity and the entrapment efficiency of the MSNP-NH_2.

Dox Loading and Functionalization of MSNP-NH_2:

To obtain Dox loaded nanobots, firstly the MSNP-NH2 (1 mg) are incubated with 1 mM solution of Dox (0.5 mL) as mentioned above. After, the particles are washed 3 times with PBS, suspended in PBS (0.9 mL) and GA (100 µL) was added, to follow the protocol for the functionalization of MSNP-NH_2 with urease as mentioned above, yielding Dox-loaded urease nanobots.

In Vitro Release of Dox from MSNP-NH_2 and urease nanobots:

To evaluate the ability of the nanobots to enhance the release of the drug in the presence of urea, Dox-loaded nanobots (2 mg mL^{-1}) were dispersed in solutions of PBS without urea and solutions containing different concentrations of urea. To compare the nanobots to the conventional MSNP-NH_2 carrier, Dox loaded MSNP-NH_2 were also placed in PBS. Then, the dispersions were placed on a thermomixer at 37 °C with 300 rpm shaking to avoid sedimentation and aliquots (100 µL) were collected every hour over the course of 6h and at 24h, refreshing the medium at every time point. The aliquots were then analysed by measuring the absorbance at 480 nm, using an Infinite M200 PRO Multimode Microplate Reader, to obtain the cumulative release profile of each system.

Optical Video Recording of nanobots and Mean-Square-Displacement (MSD) analysis:

An inverted optical microscope (Leica DMi8) with a 63x water objective was used for the observation and video recording of the nanobots movement. An aqueous solution of nanobots was placed on a glass slide and thoroughly mixed with the solutions of urea at the desired concentrations. Then, the mixture was covered using a cover slip to avoid artifacts caused by

the drifting effect. Videos of 30 s were recorded up to the first 3 minutes after performing the mixture to ensure that the analysis is performed under the same conditions. The videos were obtained using a Hamamatsu camera at a frame rate of 50 fps, under bright field.

The videos were then analysed using a Python code to obtain the tracking trajectories. Then, the MSD was calculated using the following:

$MSD(\Delta t) = \langle (x_i(t+\Delta t)-x_i(t))^2 \rangle$, (i=2, for two dimensional analysis)

The diffusion coefficient (D_e) is afterwards obtained by fitting the data to the following equation:

$MSD(\Delta t) = 4 \cdot De \cdot \Delta t$,

which is valid at small time intervals for small particles with low rotational diffusion. [53] The resulting D_e is obtained by analysing 20 particles per condition and the error represents SE.

Enzymatic Activity Evaluation: the activity of the covalently bound urease on the nanobots surface was evaluated using a commercial kit that determines the concentration ammonia generated by the Berthelot method. [61] The nanobots (0.5 mg mL^{-1}) were incubated with a range (1, 5, 25, 50 and 100 mM) of concentrations of urea for 10 minutes, to study the effect of urea concentration. The enzymatic activity was also investigated over time, by incubating the nanobots (0.5 mg mL^{-1}) with the urea solution provided with the kit for varied time periods (2.5 – 120 minutes).

Hydrodynamic radii and surface charge analysis:

A Wyatt Möbius coupled with an Atlas cell pressurization system was used to obtain the hydrodynamic radii and electrophoretic mobility of the MSNP. The equipment uses a laser with 532 nm wavelength, with a detector angle of 163.5 °, performing 3 scans over an acquisition time of 5 seconds, acquiring light scattering and electrophoretic mobility data simultaneously. Each measurement was performed at least 3 times. To analyse the nanobots' movement by DLS, aqueous solutions containing nanobots and the different concentrations of urea were introduced

in the DLS. The measurements were repeated to yield 20 data points per condition. The diffusion coefficient is obtained directly from the analysis of the scattering data on the Dynamics ® software, and the error represented is the SE.

Nanobots and Dox-loaded nanobots cytotoxicity assays:

Human epithelial cervix adenocarcinoma HeLa cells were cultured in Dulbecco's modified Eagle medium (DMEM) supplemented with Fetal Bovine Serum (10%), L-Glutamine (200 nM) and Penicillin-streptomycin (1%), in a 37 °C and 5% CO_2 atmosphere, and split every 3 days at a 1:4 ratio. For the viability assessment, cells were seeded in 96-well plates at a density of 10 000 cells per well. After 24 h, the cells were incubated with nanobots or Dox-Loaded nanobots at different concentrations for another 24 hours. The MTT was performed according to manufacturer's instructions. Briefly, a working solution of MTT (12 mM) was prepared and added to cell culture medium in a ratio of 1:10 and the cells were incubated with it for 4 hours. Afterwards, the medium was removed and the formazan crystals formed were dissolved using DMSO (50 μL). Absorbance values at 570 nm wavelength were measured using an Infinite M200 PRO Multimode Microplate Reader.

Nanobots' and Dox-loaded nanobots cytotoxicity assays:

Human epithelial cervix adenocarcinoma HeLa cells were cultured in Dulbecco's modified Eagle medium (DMEM) supplemented with Fetal Bovine Serum (10%), L-Glutamine (200 nM) and Penicillin-streptomycin (1%), in a 37 °C and 5% CO_2 atmosphere, and split every 3 days at a 1:4 ratio. For the viability assessment, cells were seeded in 96-well plates at a density of 10 000 cells per well. After 24 h, the cells were incubated with nanobots (0.05 mg mL^{-1}) or Dox-loaded nanobots in the presence of 1, 5, 25, 50, 100 and 120 mM of urea s for 24 hours. The MTT assay was then performed as described above.

Imaging of HeLa cells with Dox-loaded nanobots:

Human epithelial cervix adenocarcinoma HeLa cells were cultured in Dulbecco's modified Eagle medium (DMEM) supplemented with Fetal Bovine Serum (10%), L-Glutamine (200 nM) and Penicillin-streptomycin (1%), in a 37 °C and 5% CO_2 atmosphere, and split every 3 days at a 1:4 ratio. For the viability assessment, cells were seeded in 8-well plates at a density of 15 000 cells per well. After 24 h, the cells were incubated with Dox-loaded nanobots (0.05 mg mL^{-1}) with urea (10 mM) and without urea for 1, 4, 6 and 24 hours. After each incubation period, the cells were washed with PBS and the membranes were labeled with wheat germ agglutinin (WGA) and the nuclei with Hoescht. The cells were imaged in 3D, using an inverted optical microscope (Leica DMi8) equipped with a 63x water objective and a galvo stage, coupled with filter cubes for Rhodamine, FITC and DAPI.

Supporting Information

Supporting Information is available from the Wiley Online Library or from the author.

Acknowledgements

The research leading to these results has received funding from the European Research Council under the European Union's Seventh Framework Program (FP7/20072013)/ERC grant agreement no. 311529 (LT-NRBS). S.S. thanks the Spanish MINECO for grants CTQ2015-68879-R (MICRODIA) and CTQ2015-72471-EXP (Enzwim). A.C.H. thanks MINECO for the Severo Ochoa fellowship and T.P. thanks MINECO for the Juan de la Cierva fellowship. The authors thank A. M-López for developing the Python code for motion analysis. S.S, A.C.H. and T.P designed the experiments. A.C.H. and T.P performed the experiments and analyzed the data. A.P-J. contributed to the execution of cell assays and A.B. participated in the fabrication process. S.S, A.C.H. and T.P wrote the manuscript. All authors discussed the results and commented on the manuscript.

Received: ((will be filled in by the editorial staff))
Revised: ((will be filled in by the editorial staff))
Published online: ((will be filled in by the editorial staff))

References

[1] J. M. Rosenholm, C. Sahlgren, M. Lindén, *Nanoscale* **2010**, *2*, 1870.

[2] J. Shi, P. W. Kantoff, R. Wooster, O. C. Farokhzad, *Nat. Rev. Cancer* **2017**, *17*, 20.
[3] I. I. Slowing, J. L. Vivero-Escoto, C. Wu, V. S. Lin, *Adv. Drug Delivery Rev.* **2008**, *60*, 1278.
[4] L. K. E. A. Abdelmohsen, F. Peng, Y. Tu, D. A. Wilson, *J. Mater. Chem. B* **2014**, *2*, 2395.
[5] J. Wang, W. Gao, *ACS Nano* **2012**, *6*, 5745.
[6] F. Mou, C. Chen, Q. Zhong, Y. Yin, H. Ma, J. Guan, *ACS Appl. Mater. Interfaces* **2014**, *6*, 9897.
[7] X. Ma, K. Hahn, S. Sanchez, *J. Am. Chem. Soc.* **2015**, *137*, 49764979.
[8] D. Patra, S. Sengupta, W. Duan, H. Zhang, P. Ryan, A. Sen, *Nanoscale* **2013**, *5*, 1273.
[9] W. Gao, J. Wang, *Nanoscale* **2014**, *6*, 10486.
[10] B. E.-F. de Ávila, C. Angell, F. Soto, M. A. Lopez-Ramirez, D. F. Báez, S. Xie, J. Wang, Y. Chen, *ACS Nano* **2016**, *10*, 4997.
[11] R. Dong, Y. Hu, Y. Wu, W. Gao, B. Ren, Q. Wang, Y. Cai, *J. Am. Chem. Soc.* **2017**, *139*, 1722.
[12] M. Xuan, Z. Wu, J. Shao, L. Dai, T. Si, Q. He, *J. Am. Chem. Soc.* **2016**, *138*, 6492.
[13] X. Chen, M. Hoop, F. Mushtaq, E. Siringil, C. Hu, B. J. Nelson, S. Pané, *Appl. Mater. Today* **2017**, *9*, 37.
[14] W. Gao, D. Kagan, O. S. Pak, C. Clawson, S. Campuzano, E. Chuluun-Erdene, E. Shipton, E. E. Fullerton, L. Zhang, E. Lauga, J. Wang, *Small* **2012**, *8*, 460.
[15] M. M. Stanton, B.-W. Park, A. Miguel-López, X. Ma, M. Sitti, *Small* **2017**, *13*, 1.
[16] M. M. Stanton, B.-W. Park, D. Vilela, K. Bente, D. Faivre, M. Sitti, S. Sanchez, *ACS Nano* **2017**, DOI: 10.1021/acsnano.7b04128.
[17] M. M. Stanton, J. Simmchen, X. Ma, A. Miguel-López, S. Sánchez, *Adv. Mater. Interfaces* **2016**, *3*, 1.
[18] B. Mostaghaci, O. Yasa, J. Zhuang, M. Sitti, Adv. Sci. 2017, 4, 1700058.
[19] S. Martel, M. Mohammadi, O. Felfoul, Z. Lu, P. Pouponneau, *Int. J. Rob. Res.* **2009**, *28*, 571.
[20] R. Di Leonardo, L. Angelani, D. Dell'arciprete, G. Ruocco, V. Iebba, S. Schippa, M. P. Conte, F. Mecarini, F. De Angelis, E. Di Fabrizio, *Proc. Natl. Acad. Sci. U. S. A.* **2010**, *107*, 9541.
[21] M. Medina-Sánchez, L. Schwarz, A. K. Meyer, F. Hebenstreit, O. G. Schmidt, *Nano Lett.* **2016**, *16*, 555.
[22] X. Ma, A. C. Hortelao, T. Patiño, S. Sanchez, *ACS Nano* **2016**, *10*, 9111.
[23] J. Katuri, X. Ma, M. M. Stanton, S. Sanchez, *Acc. Chem. Res.* **2016**, *50*, 2.
[24] S. Sanchez, L. Soler, J. Katuri, *Angew. Chemie Int. Ed.* **2015**, *54*, 1414.
[25] K. K. Dey, A. Sen, *J. Am. Chem. Soc.* **2017**, *139*, 7666.
[26] V. Magdanz, G. Stoychev, L. Ionov, S. Sanchez, O. G. Schmidt, *Angew. Chemie Int. Ed.* **2014**, *53*, 2673.
[27] A. A. Solovev, W. Xi, D. H. Gracias, S. M. Harazim, C. Deneke, S. Sanchez, O. G. Schmidt, *ACS Nano* **2012**, *6*, 1751.
[28] A. A. Solovev, S. Sanchez, M. Pumera, Y. F. Mei, O. G. Schmidt, *Adv. Funct. Mater.* **2010**, *20*, 2430.
[29] S. Sanchez, A. A. Solovev, S. Schulze, O. G. Schmidt, *Chem. Commun.* **2011**, *47*, 698.
[30] W. Gao, A. Pei, R. Dong, J. Wang, *J. Am. Chem. Soc.* **2014**, *136*, 2276.
[31] X. Ma, A. Jannasch, U.-R. Albrecht, K. Hahn, A. Miguel-López, E. Schäffer, S. Sánchez, *Nano Lett.* **2015**, *15*, 7043.
[32] X. Ma, X. Wang, K. Hahn, S. Sánchez, *ACS Nano* **2016**, *10*, 3597.
[33] X. Ma, A. C. Hortelao, A. Miguel-López, S. Sánchez, *J. Am. Chem. Soc.* **2016**, *138*, 13782.
[34] L. K. E. A. Abdelmohsen, M. Nijemeisland, G. M. Pawar, G.-J. A. Janssen, R. J. M.

Nolte, J. C. M. van Hest, D. A. Wilson, *ACS Nano* **2016**, *10*, 2652.
[35] P. Schattling, B. Thingholm, B. Städler, *Chem. Mater.* **2015**, *27*, 7412.
[36] P. S. Schattling, M. A. Ramos-Docampo, V. Salgueiriño, B. Städler, *ACS Nano* **2017**, *11*, 3973.
[37] M. Nijemeisland, L. K. E. A. Abdelmohsen, W. T. S. Huck, D. A. Wilson, J. C. M. van Hest, *ACS Cent. Sci.* **2016**, *2*, 843.
[38] F. Peng, Y. Tu, A. Adhikari, J. C. J. Hintzen, D. W. P. M. Lowik, D. A. Wilson, *Chem. Commun.* **2016**, *53*, 1088.
[39] G. Rucinskaite, S. A. Thompson, S. Paterson, R. de la Rica, *Nanoscale* **2017**, *9*, 5404.
[40] Y. Tu, F. Peng, P. B. White, D. A. Wilson, *Angew. Chemie Int. Ed.* **2017**, *56*, 7620.
[41] Y. Tu, F. Peng, X. Sui, Y. Men, P. B. White, J. C. M. Van Hest, D. A. Wilson, *Nat. Chem.* **2016**, *9*, 480.
[42] Y. Tu, F. Peng, A. A. M. André, Y. Men, M. Srinivas, D. A. Wilson, *ACS Nano* **2017**, *11*, 1957.
[43] F. Tang, L. Li, D. Chen, *Adv. Mater.* **2012**, *24*, 1504.
[44] X. Ma, H. Feng, C. Liang, X. Liu, F. Zeng, Y. Wang, *J. Mater. Sci. Technol.* **2017**, DOI: 10.1016/j.jmst.2017.06.007.
[45] X. Ma, S. Sanchez, *Chem. Commun.* **2015**, *51*, 5467.
[46] X. Ma, S. Sánchez, *Tetrahedron* **2017**, *73*, 4883.
[47] W. Stober, A. Fink, *J. Colloid Interface Sci.* **1968**, *26*, 62.
[48] J. B. Sumner, D. B. Hand, *J. Am. Chem. Soc.* **1929**, *149*, 1925.
[49] P. K. Smith, R. I. Krohn, G. T. Hermanson, A. K. Mallia, F. H. Gartner, M. D. Provenzano, E. K. Fujimoto, N. M. Goeke, B. J. Olson, D. C. Klenk, *Anal. Biochem.* **1985**, *150*, 76.
[50] K. K. Dey, X. Zhao, B. M. Tansi, W. J. Méndez-Ortiz, U. M. Córdova-Figueroa, R. Golestanian, A. Sen, *Nano Lett.* **2015**, *15*, 8311.
[51] P. Gaspard, R. Kapral, **2017**, arXiv:1706.05691v1.
[52] P. Illien, R. Golestanian, A. Sen, *Chem. Soc. Rev.* **2017**, DOI: 10.1039/C7CS00087A.
[53] G. Dunderdale, S. Ebbens, P. Fairclough, J. Howse, *Langmuir* **2012**, *28*, 10997.
[54] J. R. Howse, R. A. L. Jones, A. J. Ryan, T. Gough, R. Vafabakhsh, R. Golestanian, *Phys. Rev. Lett.* **2007**, *99*, 8.
[55] Z. Bajzer, E. E. Strehler, *Biochem. Biophys. Res. Commun.* **2012**, *417*, 982.
[56] K. S. Mangaldas, Y. S. Rajput, R. Sharma, *J. Plant Biochem. Biotechnol.* **2010**, *19*, 73.
[57] D. C. Prieve, *Adv. Colloid Interface Sci.* **1999**, *82*, 93.
[58] N. Chen, C. Wu, C. Chung, Y. Hwu, S. Cheng, Y. Mou, L. Lo, *PLoS One* **2012**, *7*, 3.
[59] X. Ma, S. Jang, M. N. Popescu, W. E. Uspal, A. Miguel-López, K. Hahn, D.-P. Kim, S. Sánchez, *ACS Nano* **2016**, *10*, 8751.
[60] US Department of Health and Human Services FDA, *Use of International Standard ISO 10993-1 , " Biological evaluation of medical devices - Part 1 : Evaluation and testing within a risk management process " Guidance for Industry and Food and Drug Administration Staff*; 2016.
[61] C. J. Patton, S. R. Crouch, *Anal. Chem.* **1977**, *49*, 464.

The capability of enzyme-propelled nanomotors to enhance drug delivery is investigated in this study. Urease-powered nanomotors show active motion in ionic media and significantly improve the release of Doxorubicin in the presence of urea. The synergy between the resulting catalytic products and the enhanced drug delivery results in higher cytotoxic effect towards HeLa cells.

Nanobots, self-propulsion, enzymatic catalysis, drug delivery, nanomotors

A. C. Hortelão, T. Patiño*, A. Perez-Jiménez, À. Blanco and S. Sánchez*

Enzyme-Powered Nanobots Enhance Anticancer Drug Delivery

ToC figure (55 mm broad × 50 mm high)